Regeneration behavior of chitosan from ionic liquid using water and alcohols as anti-solvents

Xiaoyan Tan[a], Guowei Wang[a], Lei Zhong[b], Fengwei Xie[c], Ping Lan[b], Bo Chi[a,*]

[a] *College of Food Science and Light Industry, Nanjing Tech University, Nanjing, Jiangsu 211816, China*

[b] *Guangxi Key Laboratory for Polysaccharide Materials and Modification, School of Chemistry and Chemical Engineering, Guangxi University for Nationalities, Nanning, 530008, China*

[c] *International Institute for Nanocomposites Manufacturing (IINM), WMG, University of Warwick, Coventry, CV4 7AL, United Kingdom*

[*] Corresponding author. Tel.: +86 25 5813 9433; *Email:* chibo@njtech.edu.cn (B. Chi)

Abstract

While ionic liquids (ILs) have been considered as effective and "green" solvents for biopolymer processing, regeneration of IL-dissolved biopolymers could largely impact biopolymer structure and properties. This study indicates that the reconstitution of chitosan structure during regeneration from 1-ethyl-3-methylimidazolium acetate ([Emim][OAc]) depends on anti-solvent (water, methanol or ethanol) largely. Irrespective of anti-solvent, the chitosan chemical structure was not varied by dissolution or regeneration. With water, the regenerated chitosan had the highest crystallinity index of 54.18%, followed by those with methanol (35.07%) and ethanol (25.65%). Water as an anti-solvent could promote chitosan chain rearrangement, leading to the formation of an ordered aggregated structure and crystallites. Density functional theory (DFT) simulation indicated that the number of hydrogen bonds formed between anti-solvents and [Emim][OAc] was in the order of water > methanol > ethanol. With water used for regeneration, the aggregation and rearrangement of chitosan chains occurred more easily.

Keywords: Anti-solvent; Chitosan regeneration; Density functional theory; 1-Ethyl-3-methylimidazolium acetate; Ionic liquid; Molecular simulation

1. Introduction

Due to global concerns over the environmental pollutions caused by traditional, non-biodegradable synthetic polymers, natural biopolymers including polysaccharides and proteins have recently attracted huge interest in materials development. Chitosan, a copolymer of glucosamine and *N*-acetylglucosamine, is normally obtained by (in most cases, partially) deacetylation of chitin, which is the second most abundant and bio-renewable polysaccharide [1, 2]. The excellent biodegradable and biocompatible characteristics of chitosan make it widely used in areas of, for example, food preservation, separation membranes, ion-exchange resins, drug delivery systems, tissue engineering, and intelligent biosensors [3-6].

Despite its appealing properties, chitosan, like other biopolymers, is not dissolvable in water and common organic solvent systems. This is because of the inherent strong inter- and intramolecular hydrogen bonds between the hydroxyl/amino/carbonyl groups of its glucose units and its compact crystalline structure [4]. Therefore, it is indispensable to find solvents that can dissolve and manipulate chitosan effectively. Up to now, several solvent systems have been demonstrated to be capable of dissolving chitosan, such as acetic acid [7], alkali/urea system [8], *N*,*N*-dimethylacetamide (DMAc)/lithium chloride (LiCl) [9], and hexafluoro-2-propanol [10]. However, these solvent systems are generally volatile, corrosive, or toxic, and difficult to recover.

Recently, ionic liquids (ILs) have become a representative novel class of solvent for biopolymers due to their desirable characteristics such as high chemical and thermal stability, negligible vapor pressure, high versatility in chemical design, and outstanding solvation ability [11, 12]. It was found that imidazolium-based ionic liquids such as 1-butyl-3-methylimidazolium chloride ([Bmim]Cl) [13, 14], 1-allyl-3-methylimidazolium chloride ([Amim]Cl) [15, 16], 1-butyl-3-methylimidazolium acetate [Bmim][OAc] [17, 18], 1-methy-3-(3-sulfopropyl) imidazolium acetate [19], and 1-ethyl-3-methylimidazolium acetate ([Emim][OAc]) [20] are

effective at dissolving chitosan.

Regeneration is known to be the most crucial step to reconstruct dissolved polysaccharides into materials with desired properties. At present, the regeneration of polysaccharides from ILs can be performed remarkably with anti-solvents. Water, ethanol, acetone, and acetonitrile are some of the commonly used anti-solvents [21], which are miscible with ILs but not with polysaccharides, leading to significantly reduced solubility of polysaccharides in ILs. In recent years, there has been a primary focus on the regeneration of cellulose as a polysaccharide from ILs using different solvents [21-23]. In contrast, the regeneration behavior of chitosan from ILs has not been fully explored. Compressed CO_2 was reported as a gas anti-solvent to precipitate chitosan from [Bmim][OAc] solution, and the volume expansion and solvatochromic behavior of IL were studied to discuss the precipitation mechanism [5]. To the best of our knowledge, no studies have been carried out to symmetrically compare the characteristics of regenerated chitosan from ILs using different anti-solvents, not to mention the understanding of the underlying mechanisms.

Herein, we studied the regeneration of chitosan fully dissolved in [Emim][OAc] using different anti-solvents. Water, methanol, and ethanol were used as anti-solvents to precipitate chitosan and the regenerated chitosan samples were studied by structural and thermal characterization. Furthermore, density functional theory (DFT) simulation was performed to analyze the interactions between [Emim][OAc] and the anti-solvents, which provide a basis for understanding chitosan regeneration mechanisms. Our work could provide an insight into the design of effective processes based on ILs and anti-solvents for fabricating chitosan-based materials with tailored structures and properties.

2. Materials and methods

2.1 Materials

A low-viscosity grade of chitosan (≥ 90% deacetylation degree, 1.5×10^5 g/mol weight-average molecular mass) was purchased from Shanghai Ryon Biotechnology Co., Ltd (Shanghai, China). [Emim][OAc] (≥ 98% purity) was produced by the Lanzhou Institute of Chemical Physics, Chinese Academy of Sciences (Lanzhou, China). Anhydrous ethanol and methanol (analytical grade) were supplied by Sinopharm Chemical Reagent Co., Ltd (Shanghai, China). Before use, chitosan was

dried at 80 °C under vacuum for 24 h and [Emim][OAc] was kept in a vacuum oven at 90 °C for 24 h.

2.2 Dissolution and regeneration

A chitosan–[Emim][OAc] solution of 6 wt% concentration was prepared in a sealed jacketed glass vessel with magnetic stirring at 90 °C in a silicone oil bath for 5 h to ensure complete dissolution. The chitosan–[Emim][OAc] solution was clear and transparent, which was further confirmed using a polarized-light microscope (PLM).

Regenerated chitosan samples were obtained via a dissolution–coagulation route. The chitosan–[Emim][OAc] solution was poured into deionized water to obtain a coagulated chitosan hydrogel. Then the regenerated chitosan hydrogel was immersed periodically in refreshed water at room temperature for 2 days. Similarly, regenerated chitosan gels were also obtained with anhydrous ethanol or methanol, and soaked periodically in refreshed ethanol or methanol, respectively.

All the regenerated gel samples were dried in a vacuum oven at 40 °C and ground for further characterization. In the following discussion, the samples are coded as "R- CS/W", "R- CS/M", and "R- CS/E", in which "R- CS" indicates regenerated chitosan while "W", "M", and "E" represents the solvents used for regeneration, namely water, methanol, and ethanol, respectively.

2.3 Determination of molecular weight and degree of deacetylation (DD)

The molecular weight of the chitosan samples was calculated based on their intrinsic viscosities according to the Mark–Houwink–Sakurada equation [24, 25]. Chitosan was dissolved in 0.2 mol/L sodium chloride–0.1 mol/L acetic acid aqueous solution to obtain different concentration of chitosan solutions (0.05 mg/mL, 0.25 mg/mL, 0.50 mg/mL, and 0.75 mg/mL). The measurements were performed at 25 °C. The viscosity-average molecular weight (M_v) of chitosan was calculated by Eq. (1):

$$[\eta] = KM_v^{\alpha} \quad (1)$$

where [η] is the intrinsic viscosity, K and α are constants for given solute-solvent system and temperature ($K = 1.81\times10^{-3}$ and $\alpha = 0.93$), respectively.

The alkaline titration method was used to determine the degree of deacetylation (DD) of the chitosan samples [19]. Dried chitosan (0.25 g) was dissolved in 20 mL of 0.1 mol/L hydrochloric acid (HCl) with magnetic stirring. Then methyl orange was added as the indicator. Under continuous stirring, 0.1 mol/L aqueous sodium hydroxide (NaOH) was slowly added to adjust the pH of the solution. The volume of the NaOH solution added was recorded when the solution turned yellow. The DD of chitosan was calculated based on Eq. (2) and Eq. (3):

$$(\mathrm{NH_2})\% = \frac{(c_1 v_1 - c_2 v_2) \times 0.016}{m} \times 100\% \quad (2)$$

$$\mathrm{DD} = \frac{(\mathrm{NH_2})\%}{9.94\%} \times 100\% \quad (3)$$

where c_1 and c_2 are the concentrations of HCl and NaOH solutions, respectively; and v_1 and v_2 are the volumes of HCl and NaOH solutions, respectively; and m is the sample weight.

2.4 Scanning electron microscopy (SEM)

The granule morphology of chitosan was studied using a Quanta FEG 250 scanning electron microscope (FEI, USA), operated at 15.0 kV. Before a microscopic examination, the samples were sprinkled on a double-sided adhesive tape and coated with a thin layer of gold using a 108-auto sputter coater (Cressington Scientific Instruments Ltd., UK).

2.5 Attenuated total reflectance–Fourier-transform infrared (ATR-FTIR) spectroscopy

A Fourier-transform infrared (FTIR) spectrometer (Nicolet 8700, Thermo Electron Corp, Madison, WI, USA) equipped with a Nicolet Smart Orbit attenuated total reflectance (ATR) accessory and diamond internal reflection element was used to analyze the samples. The spectra were recorded in the wavenumber range of 4000–500 cm^{-1} at a resolution of 4 cm^{-1} by 64 scans. For each scanning, the spectrum was collected by subtracting the origin spectrum by the air background spectrum.

2.6 X-ray diffraction (XRD) analysis

X-ray diffraction (XRD) analysis of the samples was characterized using an X-ray

diffractometer (MiniFlex 600, Rigaku Corporation, Japan) with Cu-Kα radiation of λ = 0.1542 nm, operated at a voltage of 40 kV and a current of 40 mA. Diffractograms were collected at the diffraction angle (2θ) of 4° to 60° at room temperature with a scanning speed of 10°/min and a scanning step of 0.035°.

The crystallinity index (I_{CR}) was calculated by the following equation [26, 27]:

$$I_{CR}(\%) = \frac{I_{110} - I_{am}}{I_{110}} \times 100 \quad (4)$$

where I_{110} is the maximum intensity at about 20°, and I_{am} is the intensity of amorphous diffraction at 16°.

2.7 Small-angle X-ray scattering (SAXS) analysis

SAXS measurements were conducted on a NanoSTAR system (Bruker, Germany) equipped with a Vantec-2000 detector (active area 14[illegible] × 140 mm^2 and pixel size 68 × 68 μm^2) and a pinhole collimator for point focus geometry, operated at 50 kV and 30 W, using Cu-Kα radiation with a wavelength of 0.1542 nm as the X-ray source. The scattering vector (q) was defined as $q = 4\pi \sin\theta/\lambda$ (where 2θ is the scattering angle and λ is the wavelength of the X-ray source) [28]. The data in the region of $0.014 < q < 0.20$ Å^{-1} was used as the SAXS patterns, and was background-subtracted and normalized using the integrated Bruker software. The data analysis was done using DIFFRAC^{plus} NanoFit software.

2.8 Thermogravimetric analysis (TGA)

The thermal degradation behavior of the original and regenerated chitosan samples was determined using a thermogravimetric analyzer (STA-409PC, NETZSCH, German). The samples were loaded into alumina crucibles with a lid with a pinhole and heated from 35 °C to 750 °C at 10 °C/min under a nitrogen environment.

2.9 DFT computation

Density functional theory (DFT) simulation is a powerful method for studying inter- and intramolecular interactions on the atomic scale [29]. Here, DFT simulation was used to understand the interactions between [Emim][OAc] and anti-solvents. The maximal deviations of macroscopic and microscopic study of [Emim][OAc] and water mixtures were found to occur at approximately three water molecules per [Emim][OAc] molecule [30]. Thus, to simplify the calculation, three anti-solvent molecules were chosen for the assessment of the electronic nature of the hydrogen bond with each [Emim][OAc] molecule. The minimum energy geometries of [Emim][OAc], water, methanol, and ethanol were determined using DFT calculations. The hybrid Becke-3-Lee-Yang-Parr (B3LYP), exchange-correlation function with the 6-31+G(d,p) basis set was employed for the geometry optimizations. After that, to obtain the stable configurations of [Emim][OAc] with an anti-solvent, three optimized anti-solvent (water, methanol, or ethanol) molecules were located at several different positions around [Emim][OAc]. The minimum energy conformer was chosen as the most stable configurations of [Emim][OAc]-anti-solvent. All DFT calculations were carried out with a Gaussian 16 program (Version G16 B.01, Gaussian Inc., Wallingford CT, 2016) [31, 32].

3. Results and discussion

3.1 Molecular weight and degree of deacetylation (DD)

The molecular weight and DD values of the original and regenerated chitosan samples were summarized in **Table 1** and expressed as mean value ± standard deviation. The molecular weight and DD of the original chitosan were 1.54×10^5 g/mol and 90.24%, respectively. After dissolution and regeneration from [Emim][OAc], the regenerated chitosan samples had relatively lower molecular weight, which could be due to partial chain degradation during the course. Meanwhile, the DD of the regenerated samples increased. The molecular weight of R-CS/W (1.12×10^5 g/mol) decreased most, which might be related to chitosan hydrolysis when using water as an anti-solvent. In contrast, there were no significant differences in molecular weight and DD between R-CS/M and R-CS/E.

Table 1. Molecular weight and degree of deacetylation (DD) of the original chitosan and regenerated chitosan

samples

Sample	Molecular weight ($\times 10^5$ g/mol)	Degree of deacetylation (%)
CS	1.54 ± 0.04	90.24 ± 0.08
R-CS/W	1.12 ± 0.08	93.37 ± 0.05
R-CS/M	1.23 ± 0.03	92.13 ± 0.09
R-CS/E	1.20 ± 0.06	92.51 ±0.07

3.2 Granule morphology

Fig. 1 shows the SEM images of the original chitosan and the regenerated chitosan samples with different anti-solvents. CS displayed irregular polygon-shaped granules with a smooth and compact surface without pores. All the regenerated samples showed a conglomerate and agglomerated texture with increased surface roughness. Coagulation in water resulted in the formation of a smooth and dense surface. A relatively higher degree of smoothness was observed for R-CS/W, whereas R-CS/M and R-CS/E appeared coarse surface with flakes.

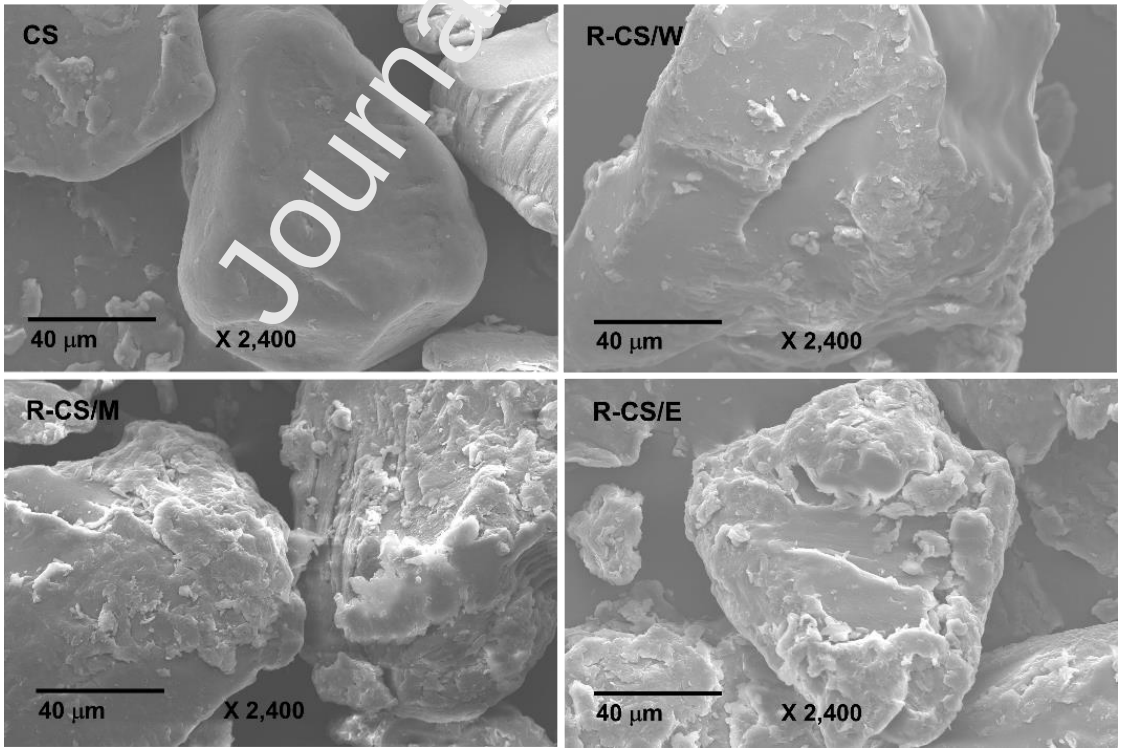

Fig. 1. SEM images of the original chitosan and regenerated chitosan samples with different anti-solvents.

3.3 Molecular chain structure

The molecular structure of chitosan after dissolution–regeneration was analyzed by FTIR spectrometry as shown in **Fig. 2**. The original chitosan showed a characteristic absorption peak at 1655 cm^{-1}, corresponding to the amide I stretching of ─CONH, while the peaks at 1588 cm^{-1} and 1319 cm^{-1} could be attributed to ─NH amide II and ─NH amide III, respectively [1, 33, 34]. The broad band in the region of 3600–3000 cm^{-1} was assigned to the overlapped stretching vibrations of ─NH_2 and ─OH groups [35]. The FTIR spectra for R-CS/W, R-CS/M, and R-CS/E all matched the functional groups of the original chitosan, with no new characteristic peaks appearing. Thus, it can be summarized that the chemical structure of chitosan remained unchanged and there was no chemical derivatization during dissolution and regeneration in [Emim][OAc]. Furthermore, the obvious characteristic FTIR absorption peak at 1567 cm^{-1} (ascribed to the asymmetric O─C─O stretches) of the anion of [Emim][OAc] [36, 37] could not be found, suggesting no residual [Emim][OAc] was left in the regenerated chitosan samples. However, there were some differences between the FTIR spectra for the original chitosan and for R-CS/W. Compared with the peak of amide II band at 1588 cm^{-1} for the original chitosan, the amide II band for R-CS/W shifted to a lower wavenumber at 1554 cm^{-1}, which might be due to chitosan recrystallization (further discussed below).

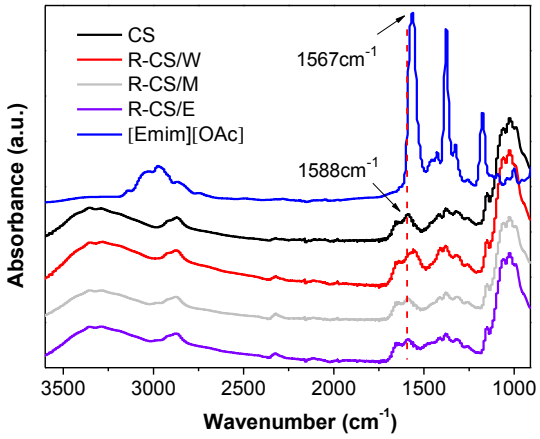

Fig. 2. FTIR spectra for [Emim][OAc], the original chitosan, and the regenerated chitosan samples with different anti-solvents.

3.4 Crystalline structure and crystallinity

XRD patterns for the original chitosan and regenerated chitosan samples with different anti-solvents are presented in **Fig. 3**. The original chitosan exhibited characteristic diffraction peaks at 2θ = 10.9° and 20.2°, corresponding to the (0 2 0) and (1 1 0) planes of the crystalline lattice of chitosan [27, 38]. All the regenerated chitosan samples displayed significantly altered X-ray diffractograms. R-CS/W displayed crystalline peaks at 2θ = 10.7°, 20.0°, 22.1°, and 26.6°. Similar XRD peaks were observed for chitosan derived from shrimp shells [27]. The XRD curve for R-CS/M showed diffraction peaks at 2θ = 20.1°, and 26.6°, along with a weak peak at about 10.9°, suggesting that a weak crystalline structure was formed during regeneration. For R-CS/E, the XRD profile revealed a dispersive broad peak at 20.3° without apparent crystalline peaks, indicating a mostly amorphous structure.

The I_{CR} value of the original chitosan was calculated to be 75.36 ± 1.44%. In comparison, the I_{CR} values of R-CS/W, R-CS/M, and R-CS/E were 54.18 ± 2.95%, 35.07 ± 3.51%, and 25.65 ± 1.09%, respectively, which are lower than that of the original chitosan. The crystallites of polysaccharides (e.g. cellulose, starch, and chitosan) could be completely destroyed during dissolution in ILs, which was correlated to their cleavage of the inter- and intramolecular hydrogen bonds [4, 37]. Then, polysaccharide chains could rearrange into an aggregated structure with the addition of an anti-solvent. Although the chitosan chains could aggregate and rearrange during the coagulation process, they could not form a better crystalline structure. As a result, the I_{CR} values of all the regenerated chitosan samples decreased. The regenerated chitosan samples showed different crystalline structures, depending on the regeneration condition. Among the regenerated samples, R-CS/W had the highest I_{CR} value, whereas R-CS/E was most amorphous. Our data here suggest that chitosan chains had a stronger tendency to rearrange into an ordered structure and form crystallites when water was used as an anti-solvent. This should be ascribed to the strong hydrogen-bonding interactions between water and [Emim][OAc], which facilitated the aggregation and rearrangement of chitosan chains. Specifically, the polarity of anti-solvent molecules is in the order of water > methanol > ethanol, so water is easier to form hydrogen bonding with [Emim][OAc] than methanol

and ethanol. Besides, the molecular size of water is smaller (followed by methanol and ethanol), providing less steric hindrance for the formation of hydrogen bonds with [Emim][OAc]. Thus, the ability of hydrogen-bonding interactions with [Emim][OAc] of the three anti-solvents should be in the sequence of water > methanol > ethanol.

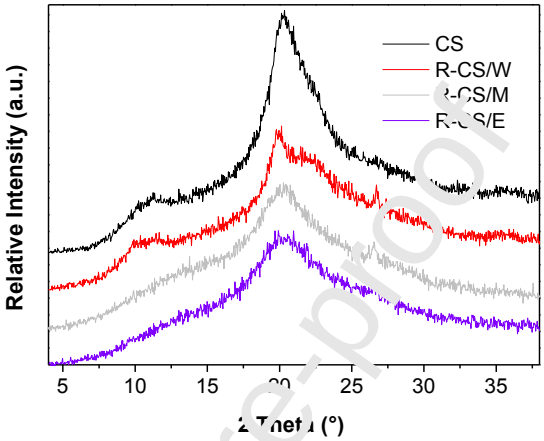

Fig. 3. X-ray diffractograms for the original chitosan and the regenerated chitosan samples with different anti-solvents.

3.5 Nano-aggregation structure

SAXS is a useful tool to analyze not only the phase behaviors of polymers in condensed and solution states, but also the perturbed or nonperiodic structures of amorphous and mesomorphic materials [39]. The aggregated structure (the ordered region and amorphous region on the nanoscale) of the regenerated chitosan samples can be studied by SAXS. **Fig. 4** exhibits the double-logarithmic SAXS patterns (a) and $I \cdot q^2$ vs. q SAXS patterns (b) of the native and regenerated chitosan samples, respectively. As seen in **Fig. 4a**, the original chitosan, as well as R-CS/W and R-CS/M, possessed a wide scattering peak in the q range of 0.03–0.14 $Å^{-1}$, implying that these samples contained an ordered aggregated structure on the nanoscale. Although the multiscale structures of chitosan were destroyed and disorganized after dissolution in [Emim][OAc], chain rearrangement during anti-solvents (water and methanol) could lead to some degree of structural order. Conversely, the scattering peak could not be observed for R-CS/E.

As shown in **Fig. 4b**, obvious scattering peaks at 0.075 $Å^{-1}$ for R-CS/W and R-CS/M were shown after the Lorentz correction [40], which should be due to the difference in electron density between the ordered and amorphous regions. Furthermore, the order degree of chitosan chains could be quantified by calculating the area ($A_q = \int_0^\infty Iq^2 dq$) under the curves in **Fig. 4b**. The integrated areas (A_q) for R-CS/W and R-CS/M were 0.072 and 0.042, respectively, whereas R-CS/E did not show any scattering peak. These results reveal that R-CS/W had the most-ordered chains, while R-CS/E possessed the minimal molecular order.

For a two-phase system polymer, SAXS scattering intensity could be influenced by the electron density difference between the ordered and amorphous regions, $\Delta\rho = \rho_o - \rho_a$ (where ρ_o and ρ_a are the electron densities of the ordered and amorphous regions of the polymer, respectively) [41]. **Fig. 4a** shows the SAXS intensity for R-CS/W was higher than those for R-CS/M and R-CS/E, while R-CS/M exhibited an intermediate level of SAXS intensity between the other two. This result reveals that the electron density difference ($\Delta\rho$) between the ordered and amorphous regions was in the sequence of R-CS/W > R-CS/M > R-CS/E, which is in agreement with the XRD results. Likely, water, because of its strong polarity and small molecular size, can interact with [Emim][OAc] more easily, facilitating the interaction between chitosan molecular chains to form the best-organized crystalline structure, as reflected by the largest ρ_o and the highest $\Delta\rho$ of R-CS/W. R-CS/M showed a lower scattering intensity and decreased $\Delta\rho$, which might be ascribed to its less ordered and less-crystalline structure. For R-CS/E, although chitosan chains rearranged into some ordered structure during coagulation, this regenerated sample had the lowest degree of crystallinity, which might result from the minimum ρ_o and $\Delta\rho$ values for this sample.

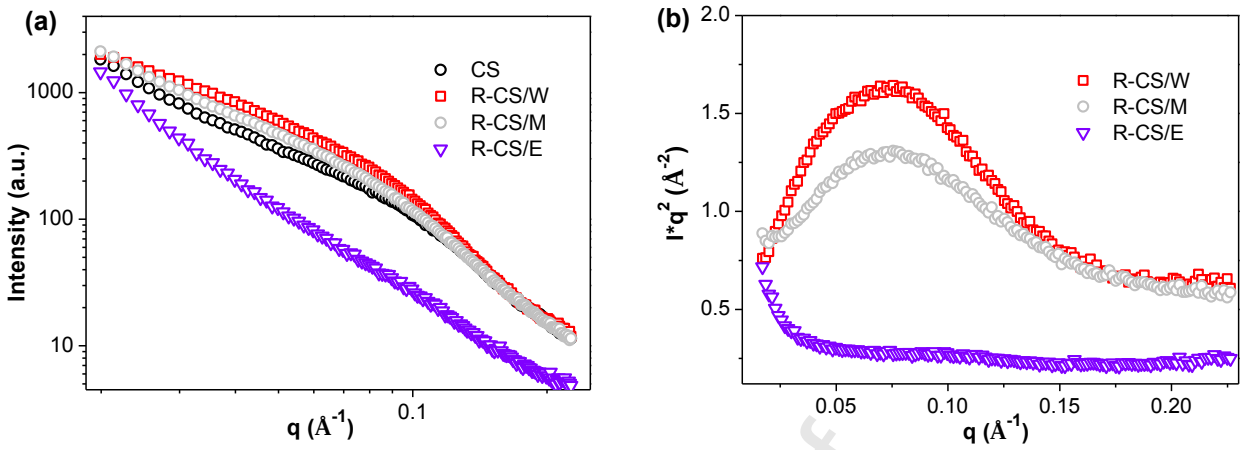

Fig. 4. Double-logarithmic SAXS patterns (a) and $I*q^2$ vs. q SAXS patterns (b) for the original chitosan and regenerated chitosan samples with different anti-solvents.

3.6 Thermal stability

TGA was used to study the thermal properties of the samples. **Fig. 5** shows the curves of weight percentage and derivative weight percentage as a function of temperature for the original chitosan and regenerated chitosan samples. The related parameters were summarized in **Table 2**. The mild weight loss of all the samples at low temperatures (<130°C) was attributed to the water evaporation process. As the temperature further increased, all the samples presented a major weight loss, which could be ascribed to the depolymerization and decomposition of chitosan. Based on previous studies, the decomposition of polysaccharide occurred by scission of glycosidic linkages first and followed by pyranose ring rupture [42, 43]. The decomposition onset temperature (T_{onset}) and peak decomposition temperature (T_{peak}) of the original chitosan were 225 °C and 302 °C, respectively. The T_{onset} values of R-CS/W, R-CS/M, and R-CS/E were 185 °C, 200 °C, and 197 °C, respectively. Thus, the regenerated chitosan samples were less thermally stable than the original chitosan, which could probably be caused by the partial chain degradation after dissolution and regeneration in [Emim][OAc]. Besides, the hydrogen bonding network and crystalline structure of regenerated chitosan could be destroyed during these processes, resulting in decreased thermal stability. The T_{peak} value of R-CS/W (297 °C) was slightly higher than that of R-CS/M (292 °C) and R-CS/E (287 °C), indicating higher thermal stability of R-CS/W. This is in agreement with the XRD and SAXS results

and indicates that water was more conducive to the formation of a hydrogen-bonding network in chitosan and the rearrangement of chitosan chains into an ordered structure.

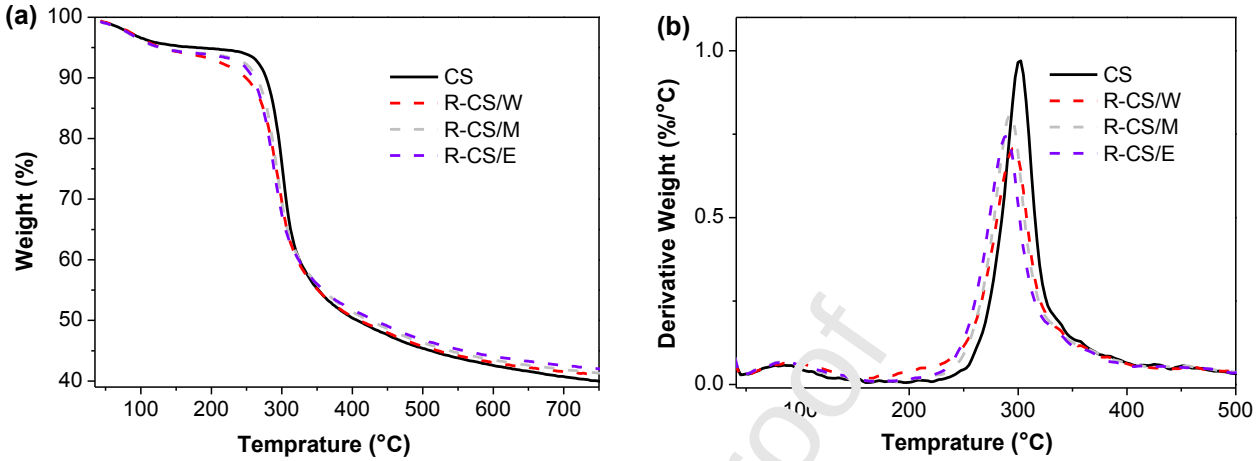

Fig. 5. Curves of weight percentage (a) and derivative weight percentage (b) as a function of temperature measured by TGA for the original chitosan and regenerated chitosan samples with different anti-solvents.

Table 2. Thermal decomposition onset temperatures (T_{onset}) and peak temperatures (T_{peak}) of the original chitosan and regenerated chitosan samples

Sample	T_{onset} (°C)	T_{peak} (°C)
CS	225	302
R-CS/W	185	297
R-CS/M	200	292
R-CS/E	197	287

3.7 DFT simulation analysis

DFT was performed by a Gaussian 16 program package at B3LYP/6-31G(d,p) level. The structure of [Emim][OAc] and different anti-solvents was optimized, and their lowest energy conformers were shown in **Fig. 6**. The molecular simulation results indicate that both $[OAc]^-$ and $[Emim]^+$ formed intermolecular hydrogen bonding with anti-solvents. The bond type and bond length values were summarized in **Table 3**. As shown in **Fig. 6** and **Table 3**, the numbers of hydrogen bonds formed between [Emim][OAc] and water, methanol, and ethanol (three anti-solvent molecules per

[Emim][OAc] molecule) were eleven, nine, and eight, respectively. In other words, the capacity of anti-solvents to form hydrogen bonds with [Emim][OAc] was in the sequence of water > methanol > ethanol. This phenomenon could be explained by the different degrees of steric hindrance provided by anti-solvents in their mixture systems. Water, due to its smaller molecular size, provides smaller steric hindrance than alcohols, which is easier to form hydrogen bonds with [Emim][OAc]. Ethanol has a bigger molecular size and provides a greater steric hindrance than methanol and thus has a weaker capacity to interact with [Emim][OAc]. Moreover, as the polarity of anti-solvent molecules is in the order of water > methanol > ethanol, the ability of these anti-solvents to form hydrogen bonds with [Emim][OAc] follows the same sequence.

The binding energy (D_0) in [Emim][OAc]–anti-solvent systems can be calculated by $D_0 = E_A + nE_B - E_{A\text{-}nB}$, where E_A, E_B, and $E_{A\text{-}nB}$ are the total energies of [Emim][OAc], anti-solvent, and the [Emim][OAc]–anti-solvent system, respectively (n is the number of anti-solvent molecules, here n = 3). The binding energy of [Emim][OAc]–3(water) was 179.61 kJ/mol, which was higher than that of [Emim][OAc]–3(methanol) (153.15 kJ/mol) and [Emim][OAc]–3(ethanol) (115.39 kJ/mol). Namely, the interaction energies of [Emim][OAc]–3(water), [Emim][OAc]–3(methanol), and [Emim][OAc]–3(ethanol) were −179.61, −153.15 and −115.39 kJ/mol, respectively. The most negative interaction energy between [Emim][OAc] and water molecules signifies the highest stability of the [Emim][OAc]–water system.

Thus, among the three solvents, water is easier to form hydrogen bonds with [Emim][OAc] and the resulting mixture system is more stable, meaning that water is the most effective anti-solvent at breaking chitosan–[Emim][OAc] hydrogen bonds and leading to the subsequent formation of chitosan–chitosan hydrogen bonding.

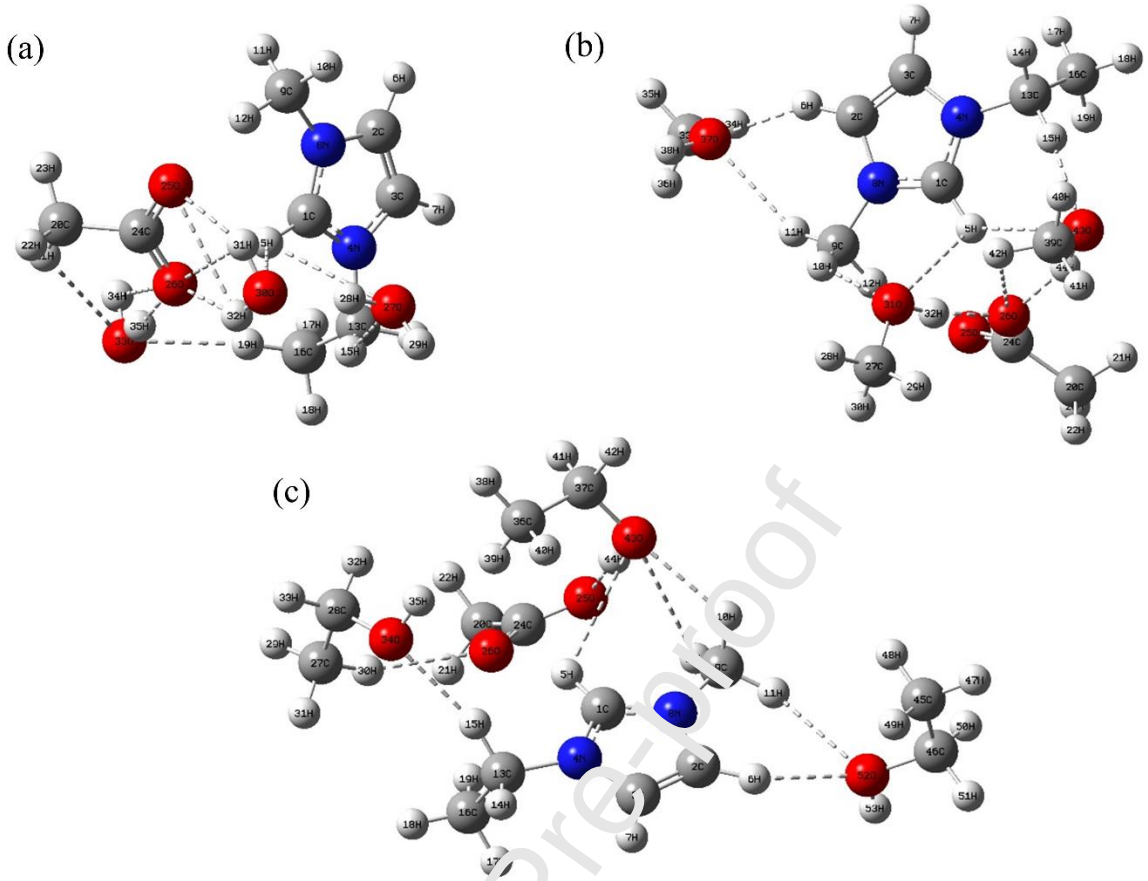

Fig. 6. Lowest energy conformers of [Emim][OAc] and anti-solvents (a, water; b, methanol; and c, ethanol) system computed based on DFT simulation. Hydrogen bonds are shown as dashed lines.

Table 3. Hydrogen bonds between [Emim][OAc] and anti-solvents.

[Emim][OAc]–water		[Emim][OAc]–methanol		[Emim][OAc]–ethanol	
A-B bond	Bond length (Å)	A-B bond	Bond length (Å)	A-B bond	Bond length (Å)
C_1—H_5· · · O_{30}	2.82	C_1—H_5· · · O_{31}	2.79	C_1—H_5· · · O_{43}	2.89009
C_1—H_5· · · O_{27}	2.96	C_1—H_5· · · O_{43}	2.84	C_2—H_6· · · O_{52}	2.25421
C_{13}—H_{15}· · · O_{27}	2.38	C_2—H_6· · · O_{37}	2.23	C_9—H_{10}· · · O_{43}	2.27243
C_{16}—H_{19}· · · O_{33}	2.34	C_9—H_{11}· · · O_{37}	2.55	C_9—H_{11}· · · O_{52}	2.55414
C_{20}—H_{21}· · · O_{33}	2.77	C_9—H_{10}· · · O_{31}	2.43	C_9—H_{12}· · · O_{43}	2.96034
O_{30}—H_{31}· · · O_{25}	1.96	C_{13}—H_{15}· · · O_{43}	2.12	C_{13}—H_{15}· · · O_{34}	2.28346
O_{30}—H_{32}· · · O_{25}	2.72	C_{39}—H_{42}· · · O_{26}	3.01	C_{27}—H_{30}· · · O_{26}	2.43712

O_{30}─H_{31}· · · O_{26}	2.65	O_{31}─H_{32}· · · O_{26}	1.72	O_{43}─H_{44}· · · O_{25}	1.69309
O_{30}─H_{32}· · · O_{26}	2.02	O_{43}─H_{44}· · · O_{26}	1.73		
O_{33}─H_{34}· · · O_{26}	3.00				
O_{33}─H_{35}· · · O_{26}	1.76				

3.8 Regeneration mechanism of chitosan from [Emim][OAc]

[Emim][OAc] can form hydrogen bonds with chitosan to disrupt its inherent strong hydrogen-bonding network and destruct its native aggregated structure. As a result, chitosan can be dissolved in [Emim][OAc] and its molecular chains are dispersed in [Emim][OAc]. By the addition of anti-solvents, chitosan can be regenerated from the chitosan-[Emim][OAc] solution without any chemical derivatization. The possible mechanism regarding the regeneration of chitosan from [Emim][OAc] with different anti-solvents is proposed in **Fig. *7***.

The above simulation results indicate that the three anti-solvents (water, methanol, and ethanol) can interact with both the $[OAc]^-$ and $[Emim]^+$ ions of the IL via hydrogen bonding. Water formed the largest number of hydrogen bonds with [Emim][OAc], leading to the easier destruction of hydrogen bonds between chitosan and [Emim][OAc] and the subsequent formation of hydrogen bonds between chitosan chains. This would facilitate chitosan chain rearrangement, responsible for the formation of an ordered aggregated structure and crystallites (shown in SAXS and XRD results), which is proposed in **Fig. 7(b)**. Ethanol, when was used as an anti-solvent, can also interact with [Emim][OAc] by hydrogen bonding, leaving chitosan chains aggregated. However, the ability of ethanol to interact with [Emim][OAc] was weaker than that of water probably due to its bigger molecular size (thus, steric hindrance) and weaker molecular polarity. As shown in **Fig. 7(c)**, with ethanol, chitosan chains can realign into a loosened aggregated structure but have less tendency to form crystallites. This corresponds to cellulose regeneration reported earlier [22]. Methanol displayed an intermediate capability of interaction with [Emim][OAc] between water and ethanol. As a consequence, the degree of order of the regenerated chitosan with methanol was also ranked in the middle. In brief, the interactions between an anti-solvent and an IL could lead to the destruction of hydrogen bonds between chitosan and the IL, and the subsequent aggregation and rearrangement of

chitosan chains. The interplay between an anti-solvent and an IL controls the structures and properties of chitosan during regeneration in ILs.

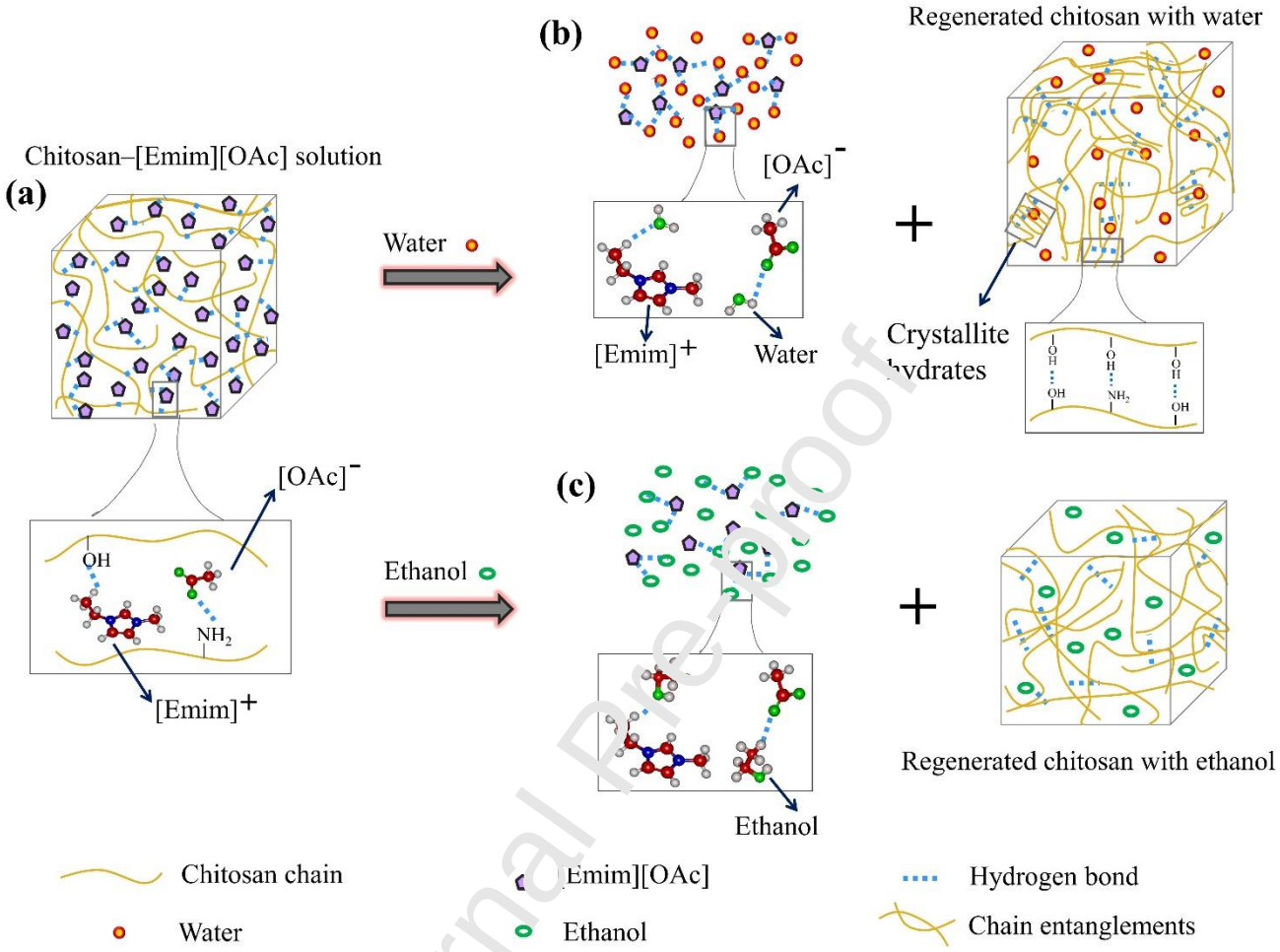

Fig. 7. Schematic representations of the regeneration of chitosan from [Emim][OAc] with water and ethanol as anti-solvents.

4. Conclusion

In this study, we systematically compared the structures and thermal stability of regenerated chitosan dissolved [Emim][OAc] by the addition of various anti-solvents (water, methanol, and ethanol). The results here reveal that anti-solvents played a crucial role in controlling the structure and property of regenerated chitosan. There was no chemical derivatization of chitosan during regeneration from [Emim][OAc]. Water, when used as an anti-solvent, could facilitate chain rearrangement and the formation of an ordered aggregated chitosan structure, leading to the relatively higher thermal stability of R-CS/W. However, when ethanol was used as an anti-solvent,

the regenerated chitosan tended to be in a disorganized and loose state. With methanol, the regenerated chitosan still contained an aggregated structure but the degree of order was less than that of the chitosan regenerated with water. The calculated I_{CR} values of R-CS/W, R-CS/M, and R-CS/E were 54.18%, 35.07%, and 25.65%, respectively. DFT simulation shows that [Emim][OAc] possesses the strongest interaction with water and the weakest with ethanol, which impacted the regeneration process of chitosan in [Emim][OAc] and resulted in the differences in the aggregated structure and properties of regenerated chitosan.

Thus, the findings from this study could guide our design of IL dissolution and regeneration processes for fabricating biopolymer materials with desired structures and properties.

Acknowledgments

The authors would like to acknowledge the Natural Science Foundation of Jiangsu Province, the National Natural Science Foundation of China (grant No. 31771049), the Foundation of Key R&D Projects of Jiangsu Province (grant No. BE2018731), and the Research Foundation of the State Key Laboratory of Materials-Oriented Chemical Engineering (grant No. ZK201806). This work is also supported by Guangxi Key Laboratory for Polysaccharide Materials and Modification, Guangxi University for Nationalities under grant No. GXPSMM18ZD-04, and Nanjing Tech University Research Start-up Grants for Introduced Talents.

References

[1] K. Juntapram, N. Praphairaksit, K. Siraleartmukul, N. Muangsin, Synthesis and characterization of chitosan-homocysteine thiolactone as a mucoadhesive polymer, Carbohydrate Polymers 87(4) (2012) 2399-2408.

[2] P.S. Bakshi, D. Selvakumar, K. Kadirvelu, N.S. Kumar, Chitosan as an environment friendly biomaterial – a review on recent modifications and applications, International Journal of Biological Macromolecules 150 (2020) 1072-1083.

[3] M.Y. Alfaifi, J. Alkabli, R.F.M. Elshaarawy, Suppressing of milk-borne pathogenic using new water-soluble chitosan-azidopropanoic acid conjugate: Targeting milk-preservation quality improvement, International Journal of Biological Macromolecules 164 (2020) 1519-1526.

[4] W. Wang, J. Zhu, X.L. Wang, Y. Huang, Y. Wang, Dissolution Behavior of Chitin in Ionic Liquids, Journal of Macromolecular Science, Part B 49(3) (2010) 528-541.

[5] X. Sun, Z. Xue, T. Mu, Precipitation of chitosan from ionic liquid solution by the compressed CO2 anti-solvent method, Green Chemistry 16(4) (2014) 2102-2106.

[6] S.S. Narasagoudr, V.G. Hegde, R.B. Chougale, S.P. Masti, S. Vootla, R.B. Malabadi, Physico-chemical and functional properties of rutin induced chitosan/poly (vinyl alcohol) bioactive films for food packaging applications, Food Hydrocolloids 109 (2020) 106096.

[7] E.A. El-Hefian, E.S. Elgannoudi, A. Mainal, A.H. Yahaya, Characterization of chitosan in acetic acid: Rheological and thermal studies, Turkish Journal of Chemistry 34(1) (2010) 47-56.

[8] J. Duan, X. Liang, Y. Cao, S. Wang, L. Zhang, High Strength Chitosan Hydrogels with Biocompatibility via New Avenue Based on Constructing Nanofibrous Architecture, Macromolecules 48(8) (2015) 2706-2714.

[9] M. Poirier, G. Charlet, Chitin fractionation and characterization in N,N-dimethylacetamide/lithium chloride solvent system, Carbohydrate Polymers 50(4) (2002) 363-370.

[10] H. Sashiwa, N. Kawasaki, A. Nakayama, E. Muraki, A. Sei-Ichi, Dissolution of Chitosan in Hexafluoro-2-propanol, Chitin & Chitosan Research 8 (2002) 249-251.

[11] M.A. Benvenuto, K.E. Gutowski, Industrial uses and applications of ionic liquids, Physical Sciences Reviews (2018) 20170191.

[12] I.C. Ferreira, D. Araújo, P. Voisin, V.D. Alves, A.A. Rosatella, C.A.M. Afonso, F. Freitas, L.A. Neves,

Chitin-glucan complex – Based biopolymeric structures using biocompatible ionic liquids, Carbohydrate Polymers 247 (2020) 116679.

[13] H. Xie, S. Zhang, S. Li, Chitin and chitosan dissolved in ionic liquids as reversible sorbents of CO2, Green Chemistry 8(7) (2006) 630-633.

[14] N.S.A. Hamid, F. Naseeruteen, W.S.W. Ngah, N. Fadilah, F.S.M. Yusof, F.B.M. Suah, Synthesis of chitin-ionic liquid beads as potential adsorbents for methylene blue, Malaysian Journal of Chemistry 22 (2020) 104-116.

[15] X. Yang, C. Zhang, C. Qiao, X. Mu, T. Li, J. Xu, L. Shi, Z. Dongju, A simple and convenient method to synthesize N-[(2-hydroxyl)-propyl-3-trimethylammonium] chitosan chloride in an ionic liquid, Carbohydrate Polymers 130 (2015) 325-332.

[16] L. Zhuang, F. Zhong, M. Qin, Y. Sun, X. Tan, H. Zhang, M. Kong, K. Hu, G. Wang, Theoretical and experimental studies of ionic liquid-urea mixtures on chitosan dissolution: Effect of cationic structure, Journal of Molecular Liquids (2020) 113918.

[17] X. Sun, Q. Tian, Z. Xue, Y. Zhang, T. Mu, The dissolution behaviour of chitosan in acetate-based ionic liquids and their interactions: from experimental evidence to density functional theory analysis, Rsc Advances 4 (2014) 30282-30291.

[18] F. Naseeruteen, N.S.A. Hamid, F.B.M. Suah, W.S.W. Ngah, F.S. Mehamod, Adsorption of malachite green from aqueous solution by using novel chitosan ionic liquid beads, International journal of biological macromolecules 107 (2018) 1270-1277.

[19] Y. Sun, M. Qing, L. Chen, J. Liu, F. Zhong, P. Jiang, G. Wang, L. Zhuang, Chitosan dissolution with sulfopropyl imidazolium Brönsted acidic ionic liquids, Journal of Molecular Liquids 293 (2019) 111533.

[20] A. Guyomard-Lack, N. Buchtová, B. Humbert, B.J. Le, Ion segregation in an ionic liquid confined within chitosan based chemical ionogels, Physical Chemistry Chemical Physics Pccp 17(37) (2015) 23947-23951.

[21] Z. Liu, X. Sun, M. Hao, C. Huang, Z. Xue, T. Mu, Preparation and characterization of regenerated cellulose from ionic liquid using different methods, Carbohydrate Polymers 117 (2015) 99-105.

[22] X. Tan, L. Chen, X. Li, F. Xie, Effect of anti-solvents on the characteristics of regenerated cellulose from 1-ethyl-3-methylimidazolium acetate ionic liquid, International Journal of Biological Macromolecules 124 (2019) 314-320.

[23] H. Artur, T. Hans, K. Tobias, Mass transport during coagulation of cellulose-ionic liquid solutions in different non-solvents, Cellulose 26 (2019) 8525-8541.

[24] R.F.M. Elshaarawy, F.H.A. Mustafa, L. van Geelen, A.E.A. Abou-Taleb, H.R.Z. Tadros, R. Kalscheuer, C. Janiak, Mining marine shell wastes for polyelectrolyte chitosan anti-biofoulants: Fabrication of high-performance economic and ecofriendly anti-biofouling coatings, Carbohydrate polymers 172 (2017) 352-364

[25] M.R. Kasaai, J. Arul, G. Charlet, Intrinsic viscosity–molecular weight relationship for chitosan, Journal of Polymer Science Part B: Polymer Physics 38(19) (2000) 2591-2598.

[26] H. El Knidri, R. El Khalfaouy, A. Laajeb, A. Addaou, A. Lahsini, Eco-friendly extraction and characterization of chitin and chitosan from the shrimp shell waste via microwave irradiation, Process Safety and Environmental Protection 104 (2016) 395-405.

[27] N.H. Marei, E.A. El-Samie, T. Salah, G.R. Saad, A.H.M. Elwahy, Isolation and characterization of chitosan from different local insects in Egypt, International Journal of Biological Macromolecules 82 (2016) 871-877.

[28] T. Suzuki, A. Chiba, T. Yarno, Interpretation of small angle x-ray scattering from starch on the basis of

fractals, Carbohydrate Polymers 34(4) (1997) 357-363.

[29] M. Qin, F. Zhong, Y. Sun, X. Tan, K. Hu, H. Zhang, M. Kong, G. Wang, L. Zhuang, Effect of cation substituent of dodecanesulfate-based anionic surface active ionic liquids on micellization: Experimental and theoretical studies, Journal of Molecular Liquids 303 (2020) 112695.

[30] C.A. Hall, K.A. Le, C. Rudaz, A. Radhi, C.S. Lovell, R.A. Damion, T. Budtova, M.E. Ries, Macroscopic and microscopic study of 1-ethyl-3-methyl-imidazolium acetate–water mixtures. The Journal of Physical Chemistry B 116(42) (2012) 12810-12818.

[31] Q. Li, J. Sun, L. Zhuang, X. Xu, Y. Sun, G. Wang, Effect of urea addition on chitosan dissolution with [Emim]Ac-Urea solution system, Carbohydrate Polymers 195 (2018) 288-297.

[32] M.J. Frisch, G.W. Trucks, H.B. Schlegel, G.E. Scuseria, M.A. Robb, J.R. Cheeseman, G. Scalmani, V. Barone, B. Mennucci, G.A. Petersson, H. Nakatsuji, M. Caricato, X. Li, H.P. Hratchian, A.F. Izmaylov, J. Bloino, G. Zheng, H.M. Sonnenberg JL, Ehara M, Toyota K, Fukuda R, Hasegawa J, Ishida M, Nakajima T, Honda Y, Kitao O, Nakai H, Vreven T, Montgomery JA, Peralta JE, Ogliaro F, Bearpark M, Heyd JJ, Brothers E, Kudin KN, Staroverov VN, Kobayashi R, Normand J, Raghavachari K, Rendell A, Burant JC, Iyengar SS, Tomasi J, Cossi M, Rega N, Millam JM, Klene M, Knox JE, Cross JB, Bakken V, Adamo C, Jaramillo J, Gomperts R, Stratmann RE, Yazyev O, Austin AJ, Cammi R, Pomennenberg C, Dapprich S, Daniels AD, Foresman JB, Ortiz JV, Cioslowski J, Fox DJ, Gaussian 16, Revision B.01, Gaussian, Inc., Wallingford CT, 2016.

[33] H.N. Abdelhamid, H.-F. Wu, Multifunctional graphene magnetic nanosheet decorated with chitosan for highly sensitive detection of pathogenic bacteria, Journal of Materials Chemistry B 1(32) (2013) 3950-3961.

[34] C. Liu, K.G.H. Desai, X. Chen, H. Park, Preparation and Characterization of Nanoparticles Containing Trypsin Based on Hydrophobically Modified Chitosan, Journal of Agricultural and Food Chemistry 53(5) (2005)

1728-1733.

[35] C. Demetgül, N. Beyazit, Synthesis, characterization and antioxidant activity of chitosan-chromone derivatives, Carbohydrate Polymers 181 (2018) 812-817.

[36] J. Sundberg, G. Toriz, P. Gatenholm, Effect of xylan content on mechanical properties in regenerated cellulose/xylan blend films from ionic liquid, Cellulose 22(3) (2015) 1943-1953.

[37] X. Tan, X. Li, L. Chen, F. Xie, Solubility of starch and microcrystalline cellulose in 1-ethyl-3-methylimidazolium acetate ionic liquid and solution rheological properties, Physical Chemistry Chemical Physics 18(39) (2016) 27584-27593.

[38] L.E. Abugoch, C. Tapia, M.C. Villamán, M. Yazdani-Pedram, M. Díaz-Dosque, Characterization of quinoa protein–chitosan blend edible films, Food Hydrocolloids 25(5) (2011) 879-886.

[39] B. Chu, B.S. Hsiao, Small-Angle X-ray Scattering of Polymers, Chemical Reviews 101(6) (2001) 1727-1762.

[40] N. Stribeck, X-ray scattering of soft matter, Springer Science & Business Media2007.

[41] X. Li, Y. He, C. Huang, J. Zhu, A.H. M. Lin, L. Chen, L. Li, Inhibition of plasticizer migration from packaging to foods during microwave heating by controlling the esterified starch film structure, Food Control 66 (2016) 130-136.

[42] L. Mdc, D.A. Aev, S.E. Mazzeto, S.D. Soares, The effect of additives on the thermal degradation of cellulose acetate, Polymer Degradation & Stability 80(1) (2003) 149-155.

[43] X. Liu, L. Yu, H. Liu, L. Chen, L. Li, Thermal Decomposition of Corn Starch with Different Amylose/Amylopectin Ratios in Open and Sealed Systems, Cereal Chemistry 86(4) (2009) 383-385.

Author statement

Xiaoyan Tan: Conceptualization, Methodology, Investigation, Writing – original draft, Writing – Review & editing. **Guowei Wang:** DFT computation, Resources. **Lei Zhong**: Data curation. **Fengwei Xie:** Writing – Review & editing, Validation. **Ping Lan:** Resources. **Bo Chi:** Conceptualization, Supervision.

Highlights

- Anti-solvents affect the structure of chitosan regenerated from ionic liquid
- Water facilitates chitosan to form ordered aggregated structure and crystallites
- Chitosan regenerated with ethanol presents mostly amorphous structure
- Water easier to form hydrogen bonds with [Emim][OAc] than alcohols